

# Metaparticles: Dressing Nano-Objects with a Hyperbolic Coating

Pan Wang,\* Alexey V. Krasavin, Francesco N. Viscomi, Ali M. Adawi, Jean-Sebastien G. Bouillard, Lei Zhang, Diane J. Roth, Limin Tong, and Anatoly V. Zayats\*

The ability to engineer the optical response of a plasmonic nano-object is highly desired to achieve better control over light–matter interactions. Due to the sensitivity of plasmon resonances to the surrounding media, isotropic dielectric coating is an easy approach to modify the optical properties of a plasmonic nanostructure. However, the choice of coatings and the provided tunability is limited by the range of refractive indices of available materials. Here, it is shown that coating of plasmonic nano-objects with an anisotropic metamaterial, which displays a hyperbolic dispersion and allows the design of refractive index on demand, provides greater flexibility in engineering their interaction with light. This is experimentally demonstrated by coating Au nanospheres with alternating SiO<sub>2</sub> and Au multishells. This creates rich and highly tunable plasmonic modes covering a broad wavelength range ( $\approx 400$ – $2200$  nm) and produces high local field intensity enhancement ( $\approx 500$ -fold). The concept is extended to hyperbolic coating of dielectric nano-objects, confirming the nature of the modes to be related to the resonances in the hyperbolic layer. The implemented approach using a coating with an engineered effective refractive index may find applications in plasmon-enhanced spectroscopy, nanolasers, design of nonlinear phenomena, photothermal conversions, and hot-electron generation.

## 1. Introduction

Localized surface plasmons are collective oscillations of a free electron gas in nanostructures, which have the ability to confine electromagnetic fields at a deep subwavelength scale, produce high local-field enhancement, and generate hot electrons.<sup>[1–3]</sup> In general, it is highly desirable that the optical properties such as scattering, absorption, or local-field distribution of a plasmonic nano-object are engineered in the required spectral range and with required values in order to achieve better performance in various applications.<sup>[4–10]</sup> For example, for plasmon-enhanced spectroscopies<sup>[4,5]</sup> or nonlinear optics,<sup>[6]</sup> the ability to tune resonance peaks and achieve strong local-field enhancement is of vital importance. In plasmon-based optical sensing, the detection limit is determined by the local fields and resonance linewidth.<sup>[7,8]</sup> At the same time, for energy harvesting, for example, in photothermal conversion and

photovoltaics, strong and broadband absorption is an important factor to be considered.<sup>[9,10]</sup>

In the past, significant efforts have been devoted to engineering the optical properties of plasmonic nano-objects.<sup>[2,11–19]</sup> These include tuning the plasmonic resonance of metal nanoparticles via material and morphology control,<sup>[11,13,14]</sup> patterning metal nanoparticles into complex coupled structures to engineer collective plasmonic modes,<sup>[15,16]</sup> using particle-on-a-mirror structures to greatly enhance the local fields,<sup>[2,17]</sup> or coupling modes in a metal nanoparticle with that in a photonic cavity for spectral narrowing.<sup>[18,19]</sup> Coating a plasmonic nano-object with an isotropic dielectric medium (Figure 1a,b) is another way to modify the optical properties,<sup>[20]</sup> which does not require precise and complex positioning, and can be easily realized in a scalable manner. However, due to the limited range of refractive indices available in conventional materials, the ability to create an essentially modified and enriched modal structure using this method is rather limited. Instead, such coating is commonly used for the stabilization of nanoparticles or as a dielectric spacer to isolate nanoparticles from their surroundings.

Electromagnetic metamaterials, artificial optical materials with engineered optical properties beyond those which could be found in nature, are attracting increasing attention since they

Dr. P. Wang, Dr. A. V. Krasavin, Dr. J.-S. G. Bouillard, Dr. D. J. Roth, Prof. A. V. Zayats

Department of Physics and London Centre for Nanotechnology  
King's College London  
Strand, London WC2R 2LS, UK

E-mail: pan.wang@kcl.ac.uk; a.zayats@kcl.ac.uk

F. N. Viscomi, Dr. A. M. Adawi, Dr. J.-S. G. Bouillard

School of Mathematics and Physical Sciences  
University of Hull

Cottingham Road, Hull HU6 7RX, UK

Dr. A. M. Adawi, Dr. J.-S. G. Bouillard

G. W. Gray Centre for Advanced Materials  
Cottingham Road, Hull HU6 7RX, UK


Prof. L. Zhang, Prof. L. M. Tong

State Key Laboratory of Modern Optical Instrumentation

College of Optical Science and Engineering

Zhejiang University

Hangzhou 310027, China

 The ORCID identification number(s) for the author(s) of this article can be found under <https://doi.org/10.1002/lpor.201800179>

DOI: 10.1002/lpor.201800179

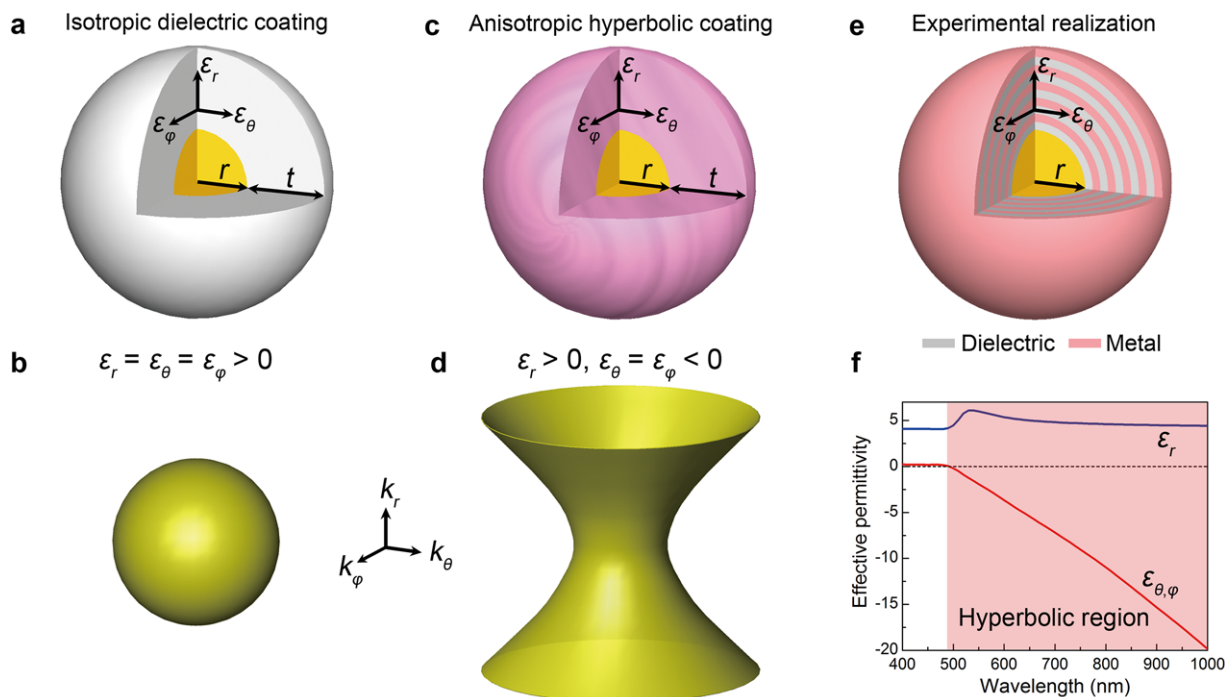


**Figure 1.** Isotropic dielectric coating versus anisotropic hyperbolic coating. Schematics of a) a plasmonic nanosphere coated with an isotropic dielectric medium and c) a homogeneous anisotropic hyperbolic medium, where  $r$  is the radius of the nanosphere,  $t$  is the thickness of the coating. Isofrequency surfaces for the b) isotropic dielectric coating ( $\epsilon_r = \epsilon_\theta = \epsilon_\phi > 0$ ) shown in (a), and d) the anisotropic hyperbolic coating ( $\epsilon_r > 0, \epsilon_\theta = \epsilon_\phi < 0$ ) shown in (c). e) Experimental realization of the hyperbolic coating in (c) with a metal–dielectric multishell coating. f) Real parts of effective permittivity of the metal–dielectric multishells in (e) determined with the effective media theory which gives a hyperbolic dispersion in the shaded wavelength range. As an example, the metallic and dielectric shells are considered as Au and SiO<sub>2</sub> shells with the same thickness.

offer a unique opportunity to observe new optical phenomena such as magnetism at high frequencies, negative refraction,<sup>[21]</sup> and superlensing<sup>[22]</sup> and open up opportunities for numerous applications in nanophotonics and nonlinear optics.<sup>[23–25]</sup> Particularly, in contrast to ordinary media, a metamaterial with an artificially created hyperbolic dispersion<sup>[26]</sup> can support optical modes with theoretically infinitely high wavevectors and, therefore, provides extremely high local density of optical states, offering the opportunity to engineer spontaneous emission rates,<sup>[27]</sup> as well as improve resolution in optical imaging.<sup>[28]</sup> Here, we show that coating of plasmonic nano-objects with a hyperbolic medium (Figure 1c,d) provides broad flexibility for designing their optical responses. The hyperbolic coating was experimentally demonstrated by coating of Au nanospheres, chosen as a classical plasmonic test object, with alternating SiO<sub>2</sub> and Au multishells. We show that a variation on the parameters of the multishells allows for the easy creation and tuning of plasmonic modes covering a broad wavelength range from 400 to 2200 nm. Theoretical calculations (in both multishell and effective medium descriptions) confirm the hyperbolic nature of the dispersion in the multishell coating and further reveal that optical properties of plasmonic nanoparticles coated with a hyperbolic metamaterial, which we term “metaparticles”, are highly dependent on the thickness of the coating, which can be tailored to a very large degree. The proposed concept was then extended to the hyperbolic coating of dielectric nanoparticles, further confirming the nature of the observed modes to be related to

the resonances in the hyperbolic layer. These results suggest an attractive way for designing optical properties of nano-objects with high tunability, broadband response, and strong local-field enhancement. It is also the first demonstration of colloidal version of hyperbolic metamaterials, which have advantages such as high flexibility in use (e.g., dispersed in solvents, spread on a surface, embedded in a solid medium) and easy excitation (e.g., by direct coupling with external illumination), and are interesting for a wide range of applications including spontaneous emission enhancement, enhanced spectroscopies, nanolasers, nonlinear optics, photothermal conversions, and hot-electron effects.

## 2. Results

### 2.1. Experimental Realization of Hyperbolic Coating

The most common implementations of hyperbolic metamaterials are nanorod arrays or layered metal–dielectric structures.<sup>[23,25–27]</sup> The latter method is particularly convenient for fabricating hyperbolic coating on various, possibly complex-shaped, nano-objects. The hyperbolic coating of colloidal metallic nanoparticles (Figure 1c) can be realized by coating them with metal–dielectric multishells (Figure 1e) using a wet chemical method.<sup>[11,29]</sup> When the multishell period is much smaller than the wavelength, the coating can be considered as an effective medium described by the anisotropic Maxwell-Garnett

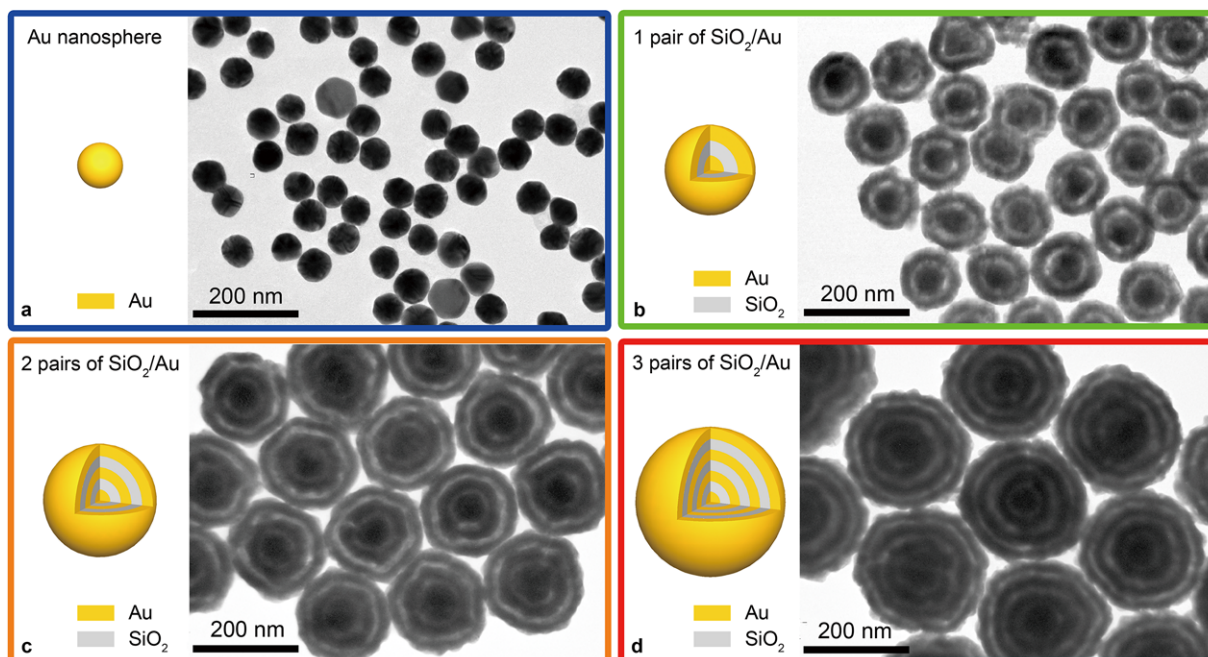


**Figure 2.** TEM images of a) uncoated Au nanospheres and metaparticles with b) one, c) two, and d) three pairs of SiO<sub>2</sub>/Au shells. The average diameter of Au nanospheres in (a) is  $\approx 62$  nm, and the average thicknesses of SiO<sub>2</sub> and Au shells in (b–d) are  $\approx 10$  and 21 nm, respectively. Insets: Corresponding schematic illustrations.

theory.<sup>[30]</sup> The permittivity tensor of such metamaterials is uniaxial in the spherical coordinate system, taking the form of  $\varepsilon_{\text{eff}} = \varepsilon_r \hat{r}\hat{r} + \varepsilon_\theta \hat{\theta}\hat{\theta} + \varepsilon_\phi \hat{\phi}\hat{\phi}$ , where  $\varepsilon_r$  and  $\varepsilon_\theta = \varepsilon_\phi = \varepsilon_t$  are the components along and perpendicular to the radial direction. The real parts of  $\varepsilon_r$  and  $\varepsilon_t$  can have different signs (Figure 1f), resulting in the characteristic hyperbolic dispersion  $k_r^2/\varepsilon_t + (k_\theta^2 + k_\phi^2)/\varepsilon_r = \omega^2/c^2$  (shown in Figure 1d as an example), where  $k_r$ ,  $k_\theta$ , and  $k_\phi$  are the components of the wavevectors of the electromagnetic wave propagating in the medium,  $\omega$  is the frequency of the wave, and  $c$  is the speed of light in vacuum.

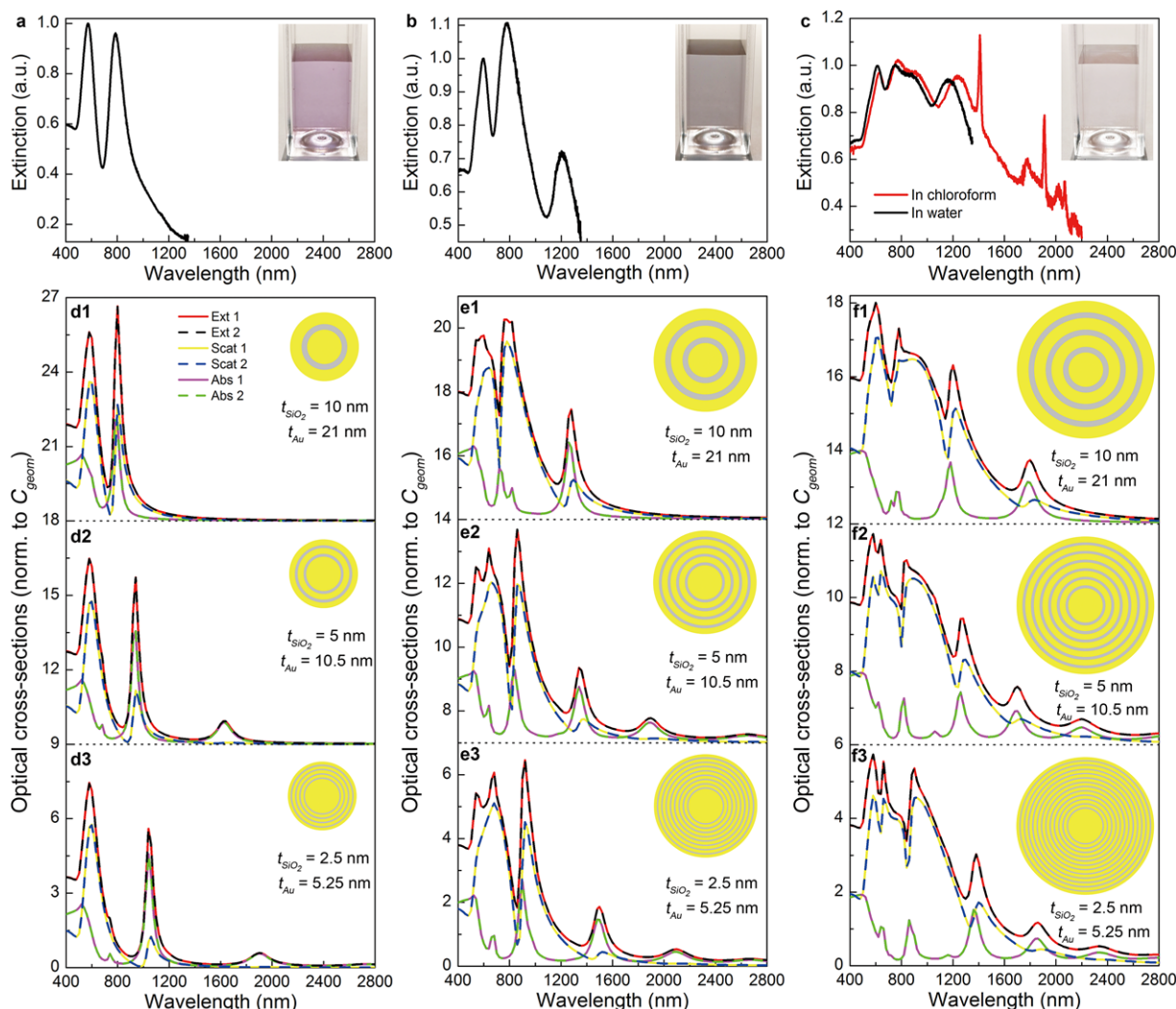
To experimentally demonstrate the feasibility of such a method, we fabricated metaparticles by alternatively coating 62-nm diameter Au nanospheres (Figure 2a) with SiO<sub>2</sub> and Au shells (see Section 4). The SiO<sub>2</sub> shell coating was realized using a modified Stöber process by controlled condensation of tetraethyl orthosilicate onto an Au surface in an alkaline environment,<sup>[31]</sup> while the Au shell coating was formed using a chemical plating method by controlled reduction of Au ions onto an Au-seed-functionalized SiO<sub>2</sub> surface.<sup>[11]</sup>

Figure 2b–d presents transmission electron microscopy (TEM) images of metaparticles with one, two, and three pairs of SiO<sub>2</sub>/Au shells, respectively, showing good uniformity in size and shape. The onion-like multishell structures (schematic illustrations in Figure 2) were clearly revealed in the TEM images, in which the Au and SiO<sub>2</sub> shells can be distinguished with a very good intensity contrast (the Au shells are darker than the SiO<sub>2</sub> shells) due to the difference in their compositions. The thicknesses of the SiO<sub>2</sub> and Au shells ( $t_{\text{SiO}_2}$  and  $t_{\text{Au}}$ ) were estimated to be about 10 and 21 nm, respectively, and can be precisely controlled during the coating processes. The average diameters of metaparticles with one, two, and three pairs of SiO<sub>2</sub>/Au shells are around 124, 186, and 248 nm, respectively.

## 2.2. Optical Properties of Metaparticles

For Au nanospheres coated with an isotropic SiO<sub>2</sub> shell (Figure S2a–c, Supporting Information), the coating causes only a slight red shift in the dipolar resonance peak (Figure S2d, Supporting Information), which is due to the small contrast in the dielectric constants of silica and the surrounding medium (water) and the strong confinement of the electric field in the vicinity of Au nanospheres (Figure S2e,f, Supporting Information). However, Au nanospheres coated with anisotropic hyperbolic metamaterial present a rich, broadband, and highly tunable plasmonic modal structure, as shown in Figure 3a–c. With an increasing number of SiO<sub>2</sub>/Au pairs, the optical properties of metaparticles change dramatically. The extinction spectrum of nanoparticles changed from having one resonance peak at 534 nm for uncoated Au nanospheres (Figure S2d, Supporting Information) to having two intense resonance peaks at 572 and 787 nm (Figure 3a) when the first pair of SiO<sub>2</sub>/Au shells was coated. Adding a second pair of SiO<sub>2</sub>/Au shells to the metaparticles induces an additional resonance around 1208 nm (Figure 3b), along with the red shift of the first peak (from 572 to 595 nm) and the blue shift of the second peak (from 787 to 776 nm). A similar behavior is observed for the metaparticles with three pairs of SiO<sub>2</sub>/Au shells (Figure 3c, black curve) with a further red shift of the first peak (from 595 to 614 nm) and blue shift of the second peak (from 776 to 751 nm). Additionally, the peak at 1208 nm, observed for the metaparticles with two pairs of SiO<sub>2</sub>/Au shells, blue-shifts to 1171 nm. Moreover, increasing the coating from two to three pairs of SiO<sub>2</sub>/Au shells enables the metaparticles to support two additional modes, at wavelengths of 875 and 1780 nm, respectively (Figure 3c). The mode at a longer wavelength is only observed when the metaparticles are transferred into chloroform (Figure 3c, red curve) to





**Figure 3.** Optical properties of metaparticles. Experimentally measured extinction spectra of metaparticles with a) one and b) two pairs of SiO<sub>2</sub>/Au shells dispersed in water, and c) three pairs of SiO<sub>2</sub>/Au shells dispersed in water (black curve) and chloroform (red curve). Insets: Corresponding photographs of the aqueous solutions of the metaparticles. d–f) Numerical simulation results: Calculated optical (absorption, scattering, and extinction) cross sections, normalized to the corresponding geometrical cross sections ( $C_{geom} = \pi(r + t)^2$ ), of the metaparticles with an overall shell thickness ( $t$ ) of d1–d3) 31 nm, e1–e3) 62 nm, and f1–f3) 93 nm, respectively. Corresponding schematics of the calculated structures and the thicknesses of silica ( $t_{SiO_2}$ ) and Au shells ( $t_{Au}$ ) are shown in the insets. Curve labels in (e) and (f) are the same as in (d). The optical cross sections (Ext1, Ext2, Scat1, Scat2, Abs1, Abs2) were calculated using various approaches detailed in Section 4.

avoid strong absorption by water molecules in the near-infrared wavelength range. In addition to the broad resonance peaks, there were also several sharp peaks around 1409, 1912, 2022, and 2071 nm in the near-infrared wavelength range (Figure 3c, red curve). These sharp peaks are due to the surface-enhanced infrared absorption of thiolated polyethylene glycol molecules absorbed on the Au shells during the fabrication process (see Section 4), as confirmed by measuring an absorption spectrum of thiolated polyethylene glycol molecules (Figure S3, Supporting Information). This result indicates high local-field enhancement in the SiO<sub>2</sub> shells between the Au shells, which will be discussed later. Dark-field scattering images and spectra of single metaparticles are presented in Figure S4, Supporting Information. The optical images clearly show well-dispersed single metaparti-

cles with color and intensity which change dramatically with the increasing number of SiO<sub>2</sub>/Au pairs. The scattering spectra are in good agreement with the corresponding extinction spectra of metaparticles. The strong scattering of single metaparticles is promising for bioimaging applications. It is worth mentioning that, compared to uncoated Au nanospheres or Au nanoshells,<sup>[32]</sup> metaparticles with three pairs of SiO<sub>2</sub>/Au shells show greatly improved sensitivity (up to 740 nm per refractive index unit) to the refractive index changes in their surrounding (Figure S5, Supporting Information), which is attractive for optical sensing applications. In addition, the resonance modes of the metaparticles can also be tuned over a wide spectral range by controlling the thickness of Au shells (Figure S6, Supporting Information).

To get an insight into the experimental observations, finite element numerical simulations of scattering of an electromagnetic wave on metaparticles were performed, and the corresponding optical cross sections were calculated (see Section 4). As shown in Figure 3d1,e1,f1, using parameters of the experimentally studied structures shown in Figure 2, the calculated extinction spectra of the metaparticles with one, two, and three pairs of  $\text{SiO}_2/\text{Au}$  shells reproduce the experimental features very well (Figure 3a–c). The much richer modal structure observed for thicker multishell coatings (Figure 3e1,f1) is due to the fact that they support higher-order modes (see the modal analysis in Section 2.4). In order to confirm the metamaterial behavior, metaparticles with increased number of  $\text{SiO}_2/\text{Au}$  pairs were also simulated by decreasing  $t_{\text{SiO}_2}$  and  $t_{\text{Au}}$ , while keeping the total coating thickness unchanged, resulting in an increased shell density. Figure 3d2,e2,f2 and Figure 3d3,e3,f3 presents the optical spectra of metaparticles with the numbers of  $\text{SiO}_2/\text{Au}$  pair two and four times of their original values (see schematics in the insets), respectively, but with the same effective permittivities. As can be clearly seen in Figure 3d1–d3, Figure 3e1–e3, and Figure 3f1–f3, with the increase in the number of  $\text{SiO}_2/\text{Au}$  pairs, when the total coating thickness is the same, the extinction spectra retain a similar shape with a general slight red shift of the peaks. Also, it can be observed that the appearance of new modes at longer wavelengths (compare Figure 3d2,d3, Figure 3e2,e3, and Figure 3f2,f3 with Figure 3d1, Figure 3e1, and Figure 3f1, respectively), is related to the extension of validity of hyperbolic dispersion to a higher wavevector region (see the discussion in Sections 2.3 and 2.4) and the consequent support of higher-order modes in the multishell coating. Thus, the rich and broadband modal structure of the nanoparticles coated with a hyperbolic metamaterial can be designed by considering a total thickness of the coating, while more precise tuning can be realized by controlling a number of  $\text{SiO}_2/\text{Au}$  pairs with the fixed coating thickness.

### 2.3. Effective Medium Description of Metal–Dielectric Multishell Coating

To further understand the nature of optical effects related to the metal–dielectric multishell coating on a plasmonic nanoparticle, numerical simulations of scattering of an electromagnetic wave on Au nanospheres coated with a layer of homogeneous hyperbolic medium were performed, and corresponding optical cross sections were calculated (see Section 4). The permittivity of the latter was evaluated using an effective medium theory (EMT), considering the experimentally measured parameters of the studied structures (Figure 2). The optical permittivity given by the EMT has a radial symmetry and possesses anisotropy, which can be expressed in a spherical coordinate system as  $\varepsilon_r = \varepsilon_{\text{Au}}\varepsilon_{\text{SiO}_2}/((1 - f_{\text{Au}})\varepsilon_{\text{Au}} + f_{\text{Au}}\varepsilon_{\text{SiO}_2})$  and  $\varepsilon_\theta = \varepsilon_\varphi = f_{\text{Au}}\varepsilon_{\text{Au}} + (1 - f_{\text{Au}})\varepsilon_{\text{SiO}_2}$ , where  $f_{\text{Au}} = t_{\text{Au}}/(t_{\text{Au}} + t_{\text{SiO}_2})$  is the Au filling factor and  $\varepsilon_{\text{Au}}$  and  $\varepsilon_{\text{SiO}_2}$  are the permittivities of Au and  $\text{SiO}_2$ . Above a certain wavelength, which depends on the filling factor, the permittivity components of the multishell coating have different signs (for the experimentally studied structures with  $f_{\text{Au}} = 0.68$ ,  $\varepsilon_\theta$  and  $\varepsilon_\varphi$  change signs from positive to negative at a wavelength of 250 nm (Figure 4a, beyond the measured wave-

length range), for  $f_{\text{Au}} = 0.5$  at a wavelength of 490 nm (Figure S7a, Supporting Information), and for  $f_{\text{Au}} = 0.32$  at a wavelength of 530 nm (Figure S8a, Supporting Information), leading to the hyperbolic dispersion of the metamaterial coating. Comparison of Figure 3d1–d3, Figure 3e1–e3, and Figure 3f1–f3 with Figure 4b, Figure 4c, and Figure 4d (calculated using the effective permittivities shown in Figure 4a), respectively, shows that with the increase of a shell density (keeping the same filling factor), the coating becomes gradually better described by the EMT. Such tendency is related to a region of the EMT applicability. The EMT can correctly describe optical modes in a metamaterial with wavevectors which are smaller than  $\sim \pi/\Lambda$ , where  $\Lambda$  is the multishell period. Thus, for the higher shell density (smaller  $\Lambda$ ), the hyperbolic dispersion given by the EMT is valid for larger wavevectors in the dispersion presented in Figure 1d and can better describe the real structure. The agreement between the optical cross sections given by the EMT and that of the multishell structure with the highest considered shell density is exceptionally good (compare Figure 4b, Figure 4c, and Figure 4d with Figure 3d3, Figure 3e3, and Figure 3f3, respectively), confirming the hyperbolic nature of the dispersion in the metal–dielectric multishell coating. The above studied case of a hyperbolic coating of a nanoparticle, which effectively creates a hyperbolic resonator formed by a metamaterial layer of a finite thickness, lays between the two extremes of a very thin hyperbolic coating and a scatterer embedded in an infinite hyperbolic medium. For thin coatings, a hyperbolic layer leads to a slight modification of the scattering properties of the nano-object, resulting in a minor red-shift of the dipolar plasmonic resonance and a change in its magnitude (Figure S7, Supporting Information). In the case of thicker coating, approaching the limit of an infinite hyperbolic medium, the nano-object scatters light into a set of propagating modes supported by the hyperbolic medium, which can be expressed through Bessel functions and vector spherical harmonics.<sup>[30]</sup>

Further exploiting the opportunities given by the EMT approach, the impact of varying metal filling factors  $f_{\text{Au}}$  (0.68, 0.5, and 0.32) on the modal structure was studied (Figure 4) (Figures S8 and S9, Supporting Information). It was found that the optical properties of the hyperbolic medium–coated Au nanospheres are quite robust with respect to the variations of a filling factor and, therefore, robust to the fabrication uncertainties of the shell thicknesses, defined mostly by the total thickness of the coating. This can be explained by the fact that the electric fields of the modes are predominantly oriented in the radial direction. Thus the modes are mostly sensitive to the radial dielectric permittivity component of the permittivity tensor, which only slightly changes with the filling factor.

### 2.4. Near-Field Intensity Distributions

In order to get further insight into the nature of the observed optical resonances and identify them, spatial distributions of the electric field intensity ( $|E|^2/|E_0|^2$ , where  $E_0$  is the incident electric field) were plotted. In contrast to uncoated or silica-coated Au nanospheres (Figure S2e,f, Supporting Information), the metaparticles with three pairs of  $\text{SiO}_2/\text{Au}$  shells possess both dipolar and quadrupolar resonances of various orders

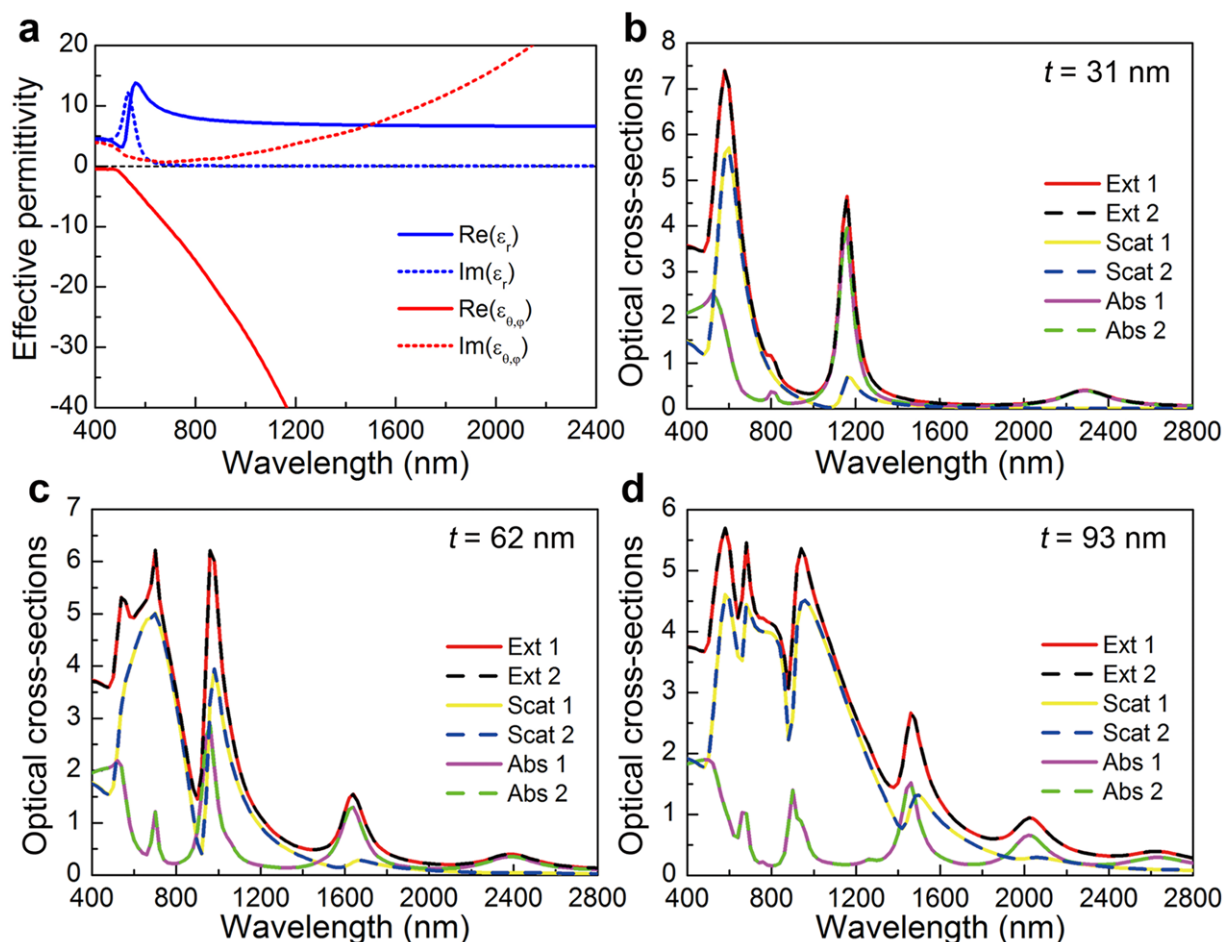


**Figure 4.** Optical properties of Au nanospheres with homogeneous hyperbolic coating. a) Effective permittivity determined using the EMT of  $\text{SiO}_2/\text{Au}$  multishells with Au filling factor ( $f_{\text{Au}}$ ) of 0.68 ( $t_{\text{SiO}_2} = 10$  nm,  $t_{\text{Au}} = 21$  nm). b–d) Numerical simulation results: Calculated optical (absorption, scattering, and extinction) cross sections, normalized to the corresponding geometrical cross sections ( $C_{\text{geom}} = \pi(r + t)^2$ ), of Au nanospheres with a homogeneous hyperbolic coating layer with the permittivity shown in (a) for coating thicknesses ( $t$ ): b) 31 nm, c) 62 nm, and d) 93 nm.

(the latter is related to the field distribution across the metamaterial layer). The nature of the short-wavelength resonance (Figure 5a1,b1,c1,d1) might be related to the excitation of bulk modes in the hyperbolic medium. Comparing the resonances of the same order, it was found that, as expected, the dipolar resonances were at the longer wavelengths than the quadrupolar ones (cf., e.g., Figure 5a5,a6 with Figure 5a2,a3,a4 and also the corresponding plots in Figure 5b,c,d). If the same type of resonance is considered (e.g., dipolar), then the higher-order resonances, both for the multilayered structures (with the field intensity localized in the outer dielectric shell) and in the EMT description, lie also at the longer wavelengths (Figure 5). A very good agreement between the intensity distributions of the resonances in the multishell structure and the one coated with the corresponding homogeneous hyperbolic medium was observed (becoming better with increasing shell density), which further confirms the feasibility of the realization of hyperbolic coating via metal–dielectric multishell coating.

The near-field distributions also allow evaluation of the electric field enhancement associated with different metaparticle resonances. As shown in Figure 5a, at the resonance conditions,

the intensity of the electric fields in the multishell structure of metaparticles with three pairs of  $\text{SiO}_2/\text{Au}$  shells is greatly enhanced. For example, the field intensity enhancements can reach the factors of  $\approx 310$ , 500, and 220 for incident light at the wavelengths of 780, 1200, and 1800 nm, respectively, which are much higher than the enhancement factor ( $\approx 50$ ) achievable with Au nanospheres (Figure S2e,f, Supporting Information). In addition, the intensity enhancement can be further increased to a maximum value of  $\approx 3000$  by increasing the shell density of the coating (Figure 5b,c), which is in a general agreement with higher field enhancement in narrower gaps in plasmonic nanostructures with the considered sizes,<sup>[33]</sup> when the non-local effects are not yet important. These results explain the experimental observation of sharp surface-enhanced infrared absorption peaks in the extinction spectrum produced by thiolated polyethylene glycol molecules absorbed on the Au shells (Figure 3c). The high and spectrally broad local-field enhancement introduced by the hyperbolic coating of plasmonic nano-objects is extremely useful for applications such as enhanced infrared and Raman spectroscopies,<sup>[34]</sup> nonlinear optics,<sup>[6]</sup> hot-electron generation,<sup>[3,35]</sup> and photothermal conversions.<sup>[36,37]</sup>



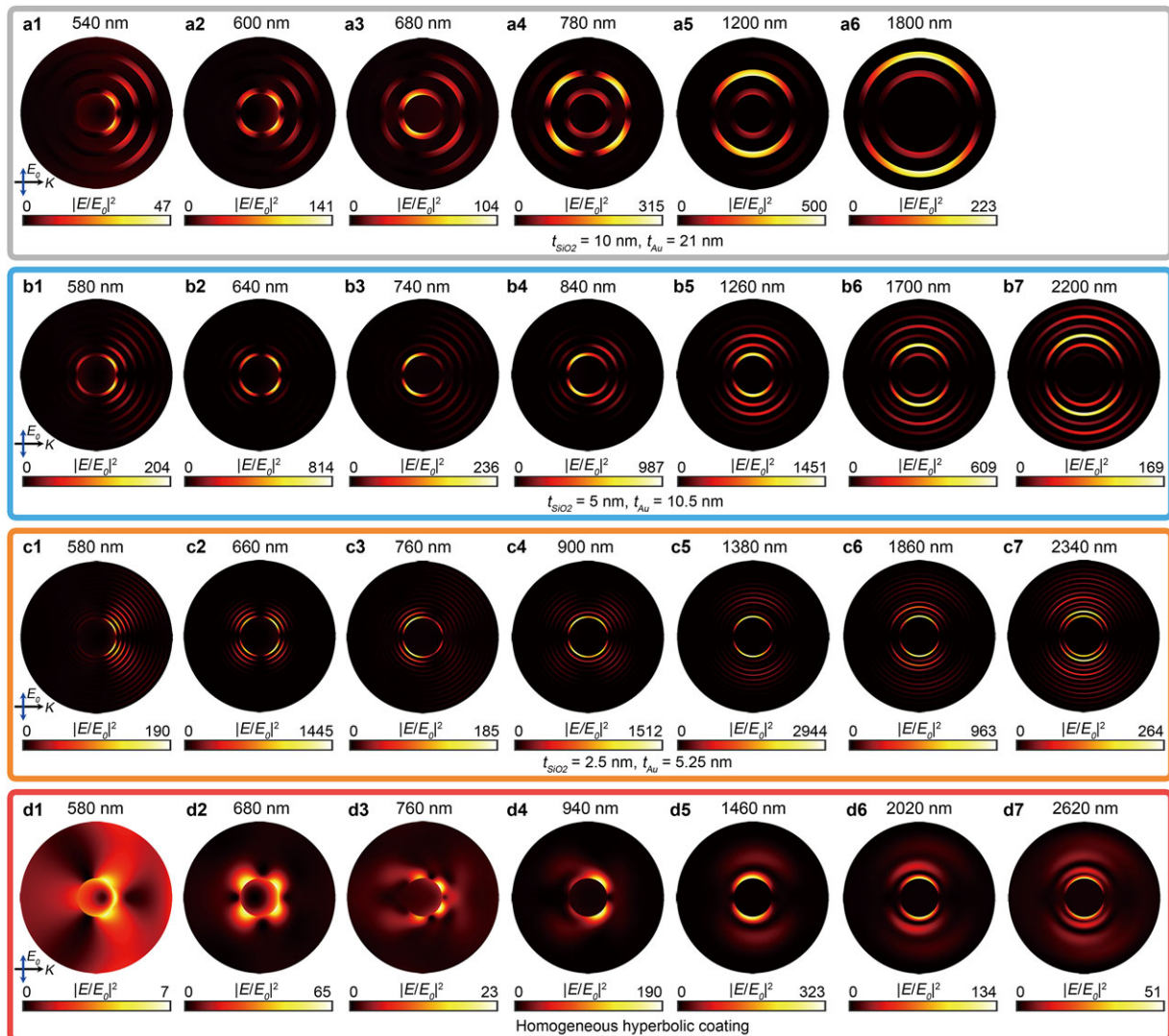


**Figure 5.** Electric field distributions in metaparticles. Electric field distributions for a metaparticle with a) 3 pairs of SiO<sub>2</sub>/Au shells ( $t_{\text{SiO}_2} = 10$  nm,  $t_{\text{Au}} = 21$  nm) plotted at the wavelengths corresponding to the resonance peaks shown in Figure 3f1, b) 6 pairs of SiO<sub>2</sub>/Au shells with two times smaller shell thicknesses ( $t_{\text{SiO}_2} = 5$  nm,  $t_{\text{Au}} = 10.5$  nm) plotted at the wavelengths corresponding to the resonance peaks shown in Figure 3f2, and c) 12 pairs of SiO<sub>2</sub>/Au shells with four times smaller thicknesses ( $t_{\text{SiO}_2} = 2.5$  nm,  $t_{\text{Au}} = 5.25$  nm) plotted at the wavelengths corresponding to the resonance peaks shown in Figure 3f3. d) Electric field distributions for an Au nanosphere coated with a layer of homogeneous hyperbolic medium with the thickness and EMT permittivity corresponding to all the designs considered above, plotted at the wavelengths corresponding to the resonance peaks shown in Figure 4d.

## 2.5. Hyperbolic Coating of Dielectric Nano-Objects

Apart from the hyperbolic coating of plasmonic nano-objects, the concept was also extended to dielectric nano-objects (Figure 6a). Figure 6 shows optical cross sections and near-field distributions of silica nanospheres coated with dielectric-metal multishells and a corresponding homogeneous hyperbolic medium (see also Figure S10, Supporting Information). A very good agreement between the two descriptions was shown, ascertaining the applicability of hyperbolic coating to modify optical response of dielectric nano-objects. It is worth noting that in the case of a dielectric core, a response similar to the metallic core case was observed (Figures 3–5). This confirms that the nature of

the modes and, therefore, the extinction spectrum of the metaparticle is essentially defined by the hyperbolic coating acting as a resonator with very high density of local electromagnetic states.

## 2.6. Applications

The hyperbolic coating of nanoparticles leads to the creation of a colloidal version of hyperbolic metamaterials. Compared with traditional hyperbolic optical metamaterials in the form of plasmonic nanorod assemblies or metal–dielectric multilayers fabricated on a substrate,<sup>[23,25–27]</sup> hyperbolic metaparticles show many

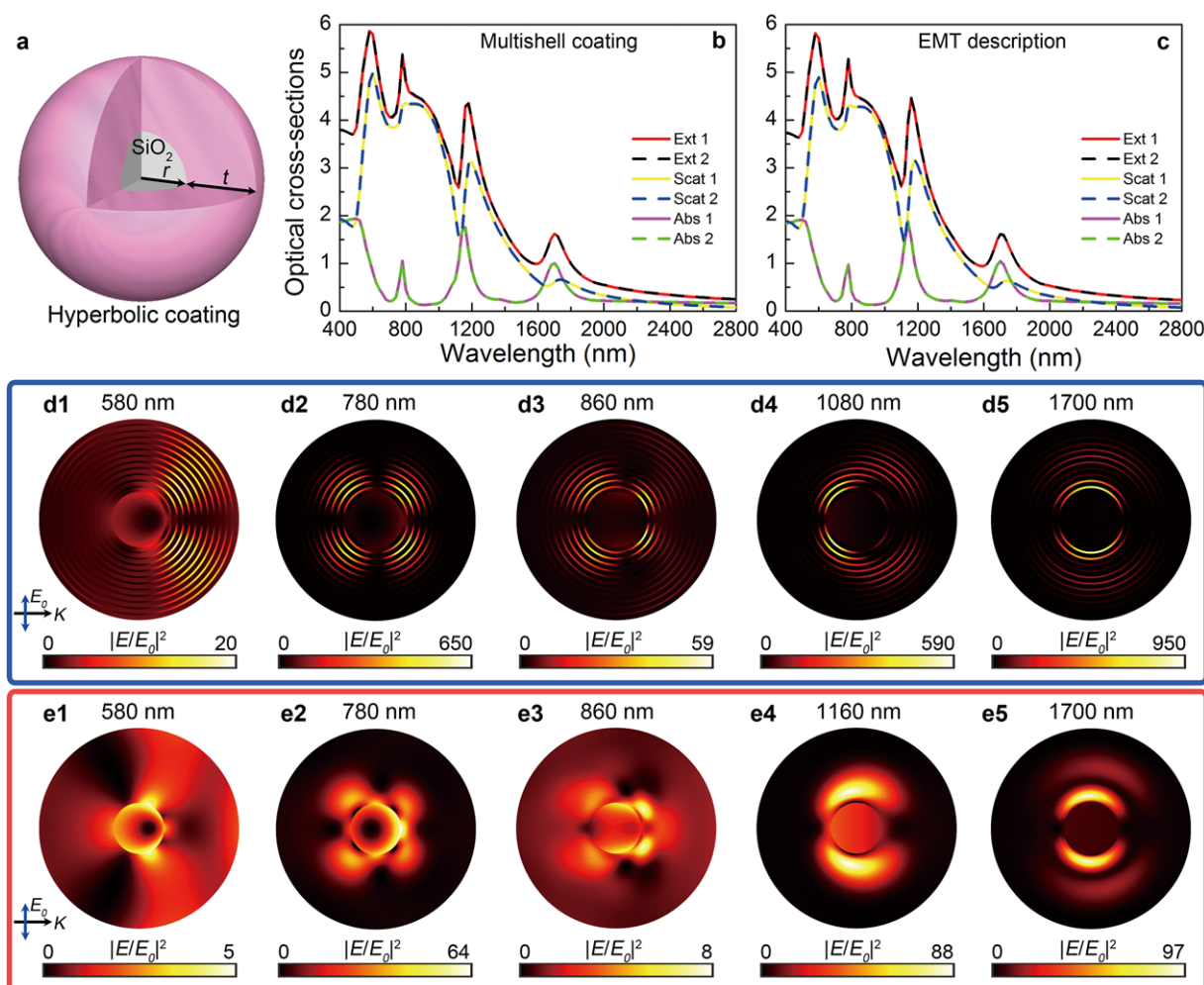


**Figure 6.** a) Schematic of an SiO<sub>2</sub> nanosphere coated with a hyperbolic medium. Calculated optical (absorption, scattering, and extinction) cross sections, normalized to the corresponding geometrical cross sections ( $C_{geom} = \pi(r + t)^2$ ), of b) an SiO<sub>2</sub> nanosphere ( $r = 31$  nm) with 12 pairs of SiO<sub>2</sub>/Au shells ( $t_{SiO_2} = 2.5$  nm,  $t_{Au} = 5.25$  nm) and c) a homogeneous hyperbolic coating layer with permittivity shown in Figure 4a for a coating thickness  $t = 93$  nm. Electric field distributions for d) an SiO<sub>2</sub> nanosphere with 12 pairs of SiO<sub>2</sub>/Au shells and e) a layer of homogeneous hyperbolic medium plotted at the wavelengths corresponding to the resonance peaks shown in (b) and (c), respectively.

interesting advantages such as high flexibility in use (e.g., dispersed in a solvent, self-assembled on a surface, or embedded in a bulk matrix) and easy excitation of hyperbolic modes (e.g., by direct scattering of external radiation). Combined with the properties demonstrated above, hyperbolic metamaterials are promising for a broad range of applications. The hyperbolic metamaterials can be used as antennas for the enhancement of spontaneous emission rate and outcoupling efficiency of embedded or external emitters<sup>[27,38–41]</sup> by directly dispersing them into an active solution or spreading them on an active surface. It is also possible to make active hyperbolic metamaterials by incorporating optical gain (dye molecules or quantum dots) directly into the dielectric shells (Figure S11, Supporting Information), opening new opportunities for developing ultra-small single-particle nanolasers.<sup>[42]</sup> In addition, single metamaterials can work as building blocks for the creation of complex hyperbolic structures via self-assembly (Figure S12, Supporting Information) which are difficult to realize using existing fabrication methods.

### 3. Conclusion

We have investigated experimentally and theoretically the dressing of a plasmonic nano-object with an anisotropic hyperbolic coating, which allows engineering the refractive index beyond that available with natural materials, leading to the creation of colloidal form of hyperbolic metamaterials. The proposed approach provides an attractive way and an additional degree of freedom for designing an optical response of a nano-object, which can be easily extended to nanoparticles made from many other materials (e.g., other metals, semiconductors, and dielectrics) and shapes (e.g., nanorods, nanocubes), or other complex nanostructures,<sup>[15]</sup> with the possibility to obtain rich and interesting optical responses. Apart from the wet chemical method demonstrated above, the hyperbolic coating can also be realized in the form of dielectric/metallic multilayers by physical vapor deposition,<sup>[23,27]</sup> which is especially useful for the coating of predesigned nanostructures on a substrate. In addition, the coating is not limited



to hyperbolic media. Other anisotropic dielectric media or media with anisotropic permeability may also hold a great interest for the engineering of optical responses of nanophotonic objects.

## 4. Experimental Section

**Fabrication of Metaparticles:** The metal–dielectric multishell coating was realized by alternately coating Au nanospheres with SiO<sub>2</sub> and Au shells. The fabrication started with 62-nm diameter Au nanospheres. The details of SiO<sub>2</sub> coating on nanoparticles with an Au outmost surface and Au coating on nanoparticles with a SiO<sub>2</sub> outmost surface are as follows:

- 1) **SiO<sub>2</sub> Coating on Nanoparticles with Au Outmost Surface.** Before SiO<sub>2</sub> coating, nanoparticles with an Au outmost surface were mixed with an aqueous solution of O-[2-(3-mercaptopropionylamino)ethyl]-O'-methylpolyethylene glycol (SH-PEG) to functionalize the Au surface with a monolayer of SH-PEG molecules. After purification with repeated centrifugations, nanoparticles were dispersed into 0.8 mL deionized (DI) water, and then mixed with 5 mL of ethanol, 2  $\mu$ L of tetraethyl orthosilicate, and 30  $\mu$ L of ammonium hydroxide solution (28% NH<sub>3</sub> in H<sub>2</sub>O). The resultant solution was stirred overnight and then washed three times with ethanol. Figure S1a,d,g, Supporting Information, shows TEM images of SiO<sub>2</sub>-coated Au, Au/(SiO<sub>2</sub>/Au)<sub>1</sub>, and Au/(SiO<sub>2</sub>/Au)<sub>2</sub> nanoparticles, respectively.
- 2) **Au Coating on Nanoparticles with SiO<sub>2</sub> Outmost Surface.** The nanoparticles with an SiO<sub>2</sub> outmost surface were first functionalized with 3-aminopropyltrimethoxysilane (APTMS) for the subsequent attachment of Au seeds. Briefly, nanoparticles in ethanol were added with excessive APTMS under vigorous stirring and the solution was stirred overnight. Then, the solution was heated to 80 °C and kept at this temperature for 1 h to enhance the attachment of APTMS molecules on SiO<sub>2</sub> surface and centrifuged four times to remove unreacted APTMS molecules.
  - 2.1 **Synthesis of Au Seeds.** Au seeds of 1–2 nm sizes were prepared using a modified method demonstrated by Duff et al.<sup>[43]</sup> Briefly, under vigorous stirring, NaOH (0.5 mL, 1 M) and tetrakis(hydroxymethyl)phosphonium chloride solution (1 mL, 68 mM) were added successively into 45 mL of water. The resultant solution was stirred for a further 5 min. Then, HAuCl<sub>4</sub> (2 mL, 25 mM) was quickly added and the solution was stirred for another 30 min. The obtained solution was aged at 4 °C for at least 2 weeks before use.
  - 2.2 **Attachment of Au Seeds to APTMS-Functionalized SiO<sub>2</sub> Surface.** In a 20-mL vial, 12 mL of Au seeds was added, followed by rapid addition of HCl (600  $\mu$ L, 0.1 M), NaCl (180  $\mu$ L, 1 M), and APTMS-functionalized nanoparticles. The solution was quickly vortexed and sonicated for 15 min. The resulting solution was incubated overnight and centrifuged three times to remove free Au seeds and dispersed in DI water. Figure S1b,e,h, Supporting Information, shows TEM images of Au-seed-attached Au/SiO<sub>2</sub>, Au/(SiO<sub>2</sub>/Au)<sub>1</sub>/SiO<sub>2</sub>, and Au/(SiO<sub>2</sub>/Au)<sub>2</sub>/SiO<sub>2</sub> nanoparticles, respectively.
  - 2.3 **Growth of Au Shell on SiO<sub>2</sub> Surface.** The coating of an Au shell on the Au-seed-attached SiO<sub>2</sub> surface was done using a plating solution as a source of Au<sup>3+</sup>. The plating solution was prepared by mixing 50 mL of water, 12.5 mg of K<sub>2</sub>CO<sub>3</sub>, and 0.75 mL of 1 wt% aqueous HAuCl<sub>4</sub> solution followed by aging at 4 °C overnight. In a typical reaction, to a 20-mL vial, 2 mL of plating solution was added, followed by the addition of an appropriate amount of Au-seed-attached nanoparticle solution. Next, 10  $\mu$ L of formaldehyde solution (36.5%–38% in H<sub>2</sub>O) was quickly added, and the resultant solution was stirred for 15 min. The thickness of the Au shell was controlled by altering the volume of Au-seed-attached nanoparticle solution in the reaction.

**Finite Element Numerical Modeling:** Numerical simulations were performed using a finite element method (COMSOL Multiphysics). The scattering from Au nanospheres coated with metal–dielectric multishells as well as with a homogeneous hyperbolic layer was studied in a scattering-field formulation with a simulation domain surrounded by a perfectly matched layer, to guarantee the absence of back-reflection from the outer domain boundaries. Dielectric constant for gold was taken from ref. [44] and extended to the infrared region using the derived Drude parameters; refractive indices for silica and surrounding water were taken as 1.45 and 1.33, respectively. The symmetry of the model was used to decrease the complexity of the simulations. The nanoparticle was placed in the center of a spherical simulation domain and all the objects were cut by two planes passing through the center of the model: one is the polarization plane of the incident linearly polarized light and the other is the plane of incidence. Finally, only one quadrant of the space between these planes was set for numerical evaluation, with the appropriate boundary conditions set on its flat edge: perfect magnetic conductor for the polarization plane and perfect electric conductor for the other one. The validity of the scattering model was checked by benchmarking it against the results for scattering of a linearly polarized plane wave on a metallic nanoparticle from analytical calculations.<sup>[45]</sup> Extinction, scattering, and absorption cross sections (normalized to the corresponding geometrical cross sections of the nanoparticles) were calculated using various independent methods: direct integration of scattering field power flow over a surface surrounding the particle ( $P_{scat}$ ), direct integration of electromagnetic losses over the nanoparticle volume ( $W_{abs}$ ) and power flow entering it ( $P_{part}$ ), as well as the optical theorem ( $P_{OT}$ ) (Ext1:  $P_{OT}$ , Ext2:  $P_{part} + P_{scat}$ , Scat1:  $P_{OT} - W_{abs}$ , Scat2:  $P_{scat}$ , Abs1:  $W_{abs}$ , Abs2:  $P_{part}$ ). The results obtained from the different methods were found to be in excellent agreement, which further confirms the validity of the model and the calculation techniques. The field maps were reconstructed over the entire space again using the symmetry of the model.

## Supporting Information

Supporting Information is available from the Wiley Online Library or from the author.

## Acknowledgements

P.W. and A.V.K. contributed equally to this work. This work was funded in part by the Engineering and Physical Sciences Research Council (UK) and the European Research Council iPLASMM project (321268). A.V.Z. acknowledges support from the Royal Society and the Wolfson Foundation.

## Conflict of Interest

The authors declare no conflict of interest.

## Keywords

coating, hyperbolic metamaterials, metaparticles, multishells, plasmonics

Received: July 2, 2018  
Revised: August 20, 2018  
Published online: October 2, 2018

[1] D. K. Gramotnev, S. I. Bozhevolnyi, *Nat. Photonics* **2010**, *4*, 83.

- [2] C. Ciraci, R. T. Hill, J. J. Mock, Y. Urzhumov, A. I. Fernández-Domínguez, S. A. Maier, J. B. Pendry, A. Chilkoti, D. R. Smith, *Science* **2012**, 337, 1072.
- [3] M. L. Brongersma, N. J. Halas, P. Nordlander, *Nat. Nanotechnol.* **2015**, 10, 25.
- [4] A. Kinkhabwala, Z. F. Yu, S. H. Fan, Y. Avlasevich, K. Müllen, W. E. Moerner, *Nat. Photonics* **2009**, 3, 654.
- [5] G. M. Akselrod, C. Argyropoulos, T. B. Hoang, C. Ciraci, C. Fang, J. Huang, D. R. Smith, M. H. Mikkelsen, *Nat. Photonics* **2014**, 8, 835.
- [6] M. Kauranen, A. V. Zayats, *Nat. Photonics* **2012**, 6, 737.
- [7] L. J. Sherry, S.-H. Chang, G. C. Schatz, R. P. Van Duyne, B. J. Wiley, Y. N. Xia, *Nano Lett.* **2005**, 5, 2034.
- [8] N. Liu, M. L. Tang, M. Hentschel, H. Giessen, A. P. Alivisatos, *Nat. Mater.* **2011**, 10, 631.
- [9] H. A. Atwater, A. Polman, *Nat. Mater.* **2010**, 9, 205.
- [10] K. Wu, J. Chen, J. R. McBride, T. Lian, *Science* **2015**, 349, 632.
- [11] S. J. Oldenburg, R. D. Averitt, S. L. Westcott, N. J. Halas, *Chem. Phys. Lett.* **1998**, 288, 243.
- [12] C. De Angelis, A. Locatelli, D. Modotto, S. Boscolo, M. Midrio, A. D. Capobianco, *J. Opt. Soc. Am. B* **2010**, 27, 997.
- [13] C. Radloff, N. J. Halas, *Nano Lett.* **2004**, 4, 1323.
- [14] H. J. Chen, L. Shao, Q. Li, J. F. Wang, *Chem. Soc. Rev.* **2013**, 42, 2679.
- [15] J. A. Fan, C. Wu, K. Bao, J. M. Bao, R. Bardhan, N. J. Halas, V. N. Manoharan, P. Nordlander, G. Shvets, F. Capasso, *Science* **2010**, 328, 1135.
- [16] W. Zhou, T. W. Odom, *Nat. Nanotechnol.* **2011**, 6, 423.
- [17] D. Y. Lei, A. I. Fernández-Domínguez, Y. Sonnefraud, K. Appavoo, R. F. Haglund, Jr., J. B. Pendry, S. A. Maier, *ACS Nano* **2012**, 6, 1380.
- [18] M. A. Schmidt, D. Y. Lei, L. Wondraczek, V. Nazabal, S. A. Maier, *Nat. Commun.* **2012**, 3, 1108.
- [19] P. Wang, Y. P. Wang, Z. Y. Yang, X. Guo, X. Lin, X. -C. Yu, Y. -F. Xiao, W. Fang, L. Zhang, G. W. Lu, Q. H. Gong, L. M. Tong, *Nano Lett.* **2015**, 15, 7581.
- [20] Y. Lu, Y. D. Yin, Z. Y. Li, Y. N. Xia, *Nano Lett.* **2002**, 2, 785.
- [21] D. R. Smith, J. B. Pendry, M. C. K. Wiltshire, *Science* **2004**, 305, 788.
- [22] J. B. Pendry, *Phys. Rev. Lett.* **2000**, 85, 3966.
- [23] X. D. Yang, J. Yao, J. Rho, X. B. Yin, X. Zhang, *Nat. Photonics* **2012**, 6, 450.
- [24] O. Hess, J. B. Pendry, S. A. Maier, R. F. Oulton, J. M. Hamm, K. L. Tsakmakidis, *Nat. Mater.* **2012**, 11, 573.
- [25] L. H. Nicholls, F. J. Rodríguez-Fortuño, M. E. Nasir, R. M. Córdova-Castro, N. Olivier, G. A. Wurtz, A. V. Zayats, *Nat. Photonics* **2017**, 11, 628.
- [26] A. Poddubny, I. Iorsh, P. Belov, Y. Kivshar, *Nat. Photonics* **2013**, 7, 948.
- [27] D. Lu, J. J. Kan, E. E. Fullerton, Z. W. Liu, *Nat. Nanotechnol.* **2014**, 9, 48.
- [28] Z. W. Liu, H. Lee, Y. Xiong, C. Sun, X. Zhang, *Science* **2007**, 315, 1686.
- [29] E. Prodan, C. Radloff, N. J. Halas, P. Nordlander, *Science* **2003**, 302, 419.
- [30] C. Wu, A. Salandrino, X. J. Ni, X. Zhang, *Phys. Rev. X* **2014**, 4, 021015.
- [31] W. Stöber, A. Fink, E. J. Bohn, *J. Colloid Interface Sci.* **1968**, 26, 62.
- [32] S. Lal, S. Link, N. J. Halas, *Nat. Photonics* **2007**, 1, 641.
- [33] H. X. Xu, *Phys. Rev. B* **2005**, 72, 073405.
- [34] D.-K. Lim, K.-S. Jeon, H. M. Kim, J.-M. Nam, Y. D. Suh, *Nat. Mater.* **2010**, 9, 60.
- [35] P. Wang, A. V. Krasavin, M. E. Nasir, W. Dickson, A. V. Zayats, *Nat. Nanotechnol.* **2018**, 13, 159.
- [36] G. Baffou, R. Quidant, *Laser Photonics Rev.* **2013**, 7, 171.
- [37] L. J. Meng, R. W. Yu, M. Qiu, F. J. García de Abajo, *ACS Nano* **2017**, 11, 7915.
- [38] C. Guclu, T. S. Luk, G. T. Wang, F. Capolino, *Appl. Phys. Lett.* **2014**, 105, 123101.
- [39] A. P. Slobozhanyuk, P. Ginzburg, D. A. Powell, I. Iorsh, A. S. Shalin, P. Segovia, A. V. Krasavin, G. A. Wurtz, V. A. Podolskiy, P. A. Belov, A. V. Zayats, *Phys. Rev. B* **2015**, 92, 195127.
- [40] D. Lu, H. L. Qian, K. W. Wang, H. Shen, F. F. Wei, Y. F. Jiang, E. E. Fullerton, P. K. L. Yu, Z. W. Liu, *Adv. Mater.* **2018**, 30, 1706411.
- [41] C. Ayala-Orozco, J. G. Liu, M. W. Knight, Y. M. Wang, J. K. Day, P. Nordlander, N. J. Halas, *Nano Lett.* **2014**, 14, 2926.
- [42] M. J. Wan, P. Gu, W. Y. Liu, Z. Chen, Z. L. Wang, *Appl. Phys. Lett.* **2017**, 110, 031103.
- [43] D. G. Duff, A. Baiker, *Langmuir* **1993**, 9, 2301.
- [44] P. B. Johnson, R. W. Christy, *Phys. Rev. B* **1972**, 6, 4370.
- [45] J. Parsons, C. P. Burrows, J. R. Sambles, W. L. Barnes, *J. Mod. Opt.* **2010**, 57, 356.